Wind Tunnel Measurements of Non-Dimensional Lift Coefficient of a Boomerang and Comparison to Theory

Justin Tahmassebpur,[1]
University of California at San Diego, La Jolla, California 92093, USA

Martin Laslett,[2]
Quanta Training Ltd., Worchester, United Kingdom

Manuel Schütz,[3]
WKS KV Bern, Bern 3001, Switzerland

and

Prasad Gudem,[4]
University of California at San Diego, La Jolla, California 92093, USA

Abstract

In this paper, we measure the non-dimensional lift coefficient of a boomerang in a wind tunnel for various rotational speeds, translational speeds, and angles-of-incidence and we compare the measurements with the theoretical work of Hess, Vassberg, and Gudem. Hess's analysis in the 1970s predicts that the non-dimensional lift coefficient is approximately proportional to the *square* of the non-dimensional rotational speed. Vassberg's analysis in 2012 predicts that the non-dimensional lift coefficient is approximately proportional to a *constant plus the square* of the non-dimensional rotational speed. Gudem's analysis in 2019 predicts that the non-dimensional lift coefficient is approximately *linearly* proportional to the non-dimensional rotational speed due to the reversal of airflow and the reversal of angle-of-attack as the blades traverse the 360^0 angles of rotation. Comparison of wind tunnel measurement results with the theoretical predictions shows that the non-dimensional lift coefficient is indeed *linearly* proportional to the non-dimensional rotational speed, consistent with Gudem's theoretical predictions.

[1] Undergraduate student, Department of Electrical and Computer Engineering
[2] IT Trainer, Technical IT Group
[3] Grammar School Teacher in Physics and Mathematics
[4] Adjunct Professor, Department of Electrical and Computer Engineering

Nomenclature

C = Chord length (m)

C_{l0+} = Basic lift coefficient for leading edge

C_{l0-} = Basic lift coefficient for trailing edge

$C_{l\alpha+}$ = Lift coefficient due to angle of attack for leading edge (per rad)

$C_{l\alpha-}$ = Lift coefficient due to angle of attack for trailing edge (per rad)

$\overline{C_l}$ = Non-dimensional lift coefficient

L_0 = Basic lift (N)

L_0^+ = Basic lift for leading edge (N)

L_0^- = Basic lift for trailing edge (N)

L_α = Lift due to angle-of-attack (N)

L_α^+ = Lift due to angle-of-attack for leading edge (N)

L_α^- = Lift due to angle-of-attack for trailing edge (N)

r = Radial coordinate (m)

R = Blade length (m)

α_{AOA} = Angle-of-attack (rad)

α_p = Blade pitch (rad)

α_{pi+} = Inherent blade pitch for the leading edge (rad)

α_{pi-} = Inherent blade pitch for the trailing edge (rad)

α_{AOI} = Angle-of-incidence (rad)

V_{no} = Basic normal velocity of the wind (m/s)

$V_{n\alpha}$ = Attack normal velocity of the wind (m/s)

L_p^+ = Nondimensional integral over leading edge for lift due to blade pitch

L_p^- = Nondimensional integral over trailing edge for lift due to blade pitch

L_{AOI}^+ = Nondimensional integral over leading edge for lift due to angle-of-incidence

L_{AOI}^- = Nondimensional integral over trailing edge for lift due to angle-of-incidence

ψ = Euler angle between N-axis and X-axis (rad)

ρ = Air density (kg/m^3)

χ = Non-dimensional rotational speed of the blade tip $\left(\frac{R\omega}{V}\right)$

ω = Rotational velocity (rad/s)

I. Introduction

The boomerang is mankind's oldest flying machine that still fascinates scientists and layman. Returning boomerang was invented and used in Australia for thousands of years. It was discovered only a few hundred years ago by visitors to Australia from the rest of the world. Since then, the returning boomerang has developed into many variants, but the most enthusiastic throwers are from the sport of competitive boomerang throwing and catching, where some remarkable feats of technology and athleticism have been achieved. As shown in Fig. 1, an amazing variety of boomerang shapes have evolved by trial and error to meet the demands of boomerang competition without complete understanding of the underlying science.

.

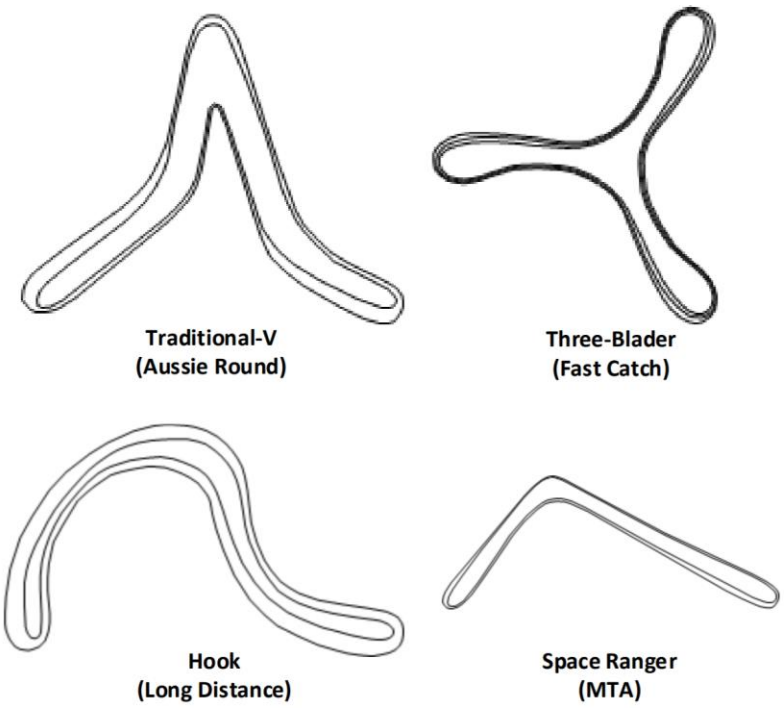

Figure 1: Sample of Boomerangs Used in Competitive Championships

In the 1970's Felix Hess developed a set of aerodynamic equations describing the flight trajectory of a boomerang [1]. He gathered experimental data from different boomerang shapes and initial conditions and compared the results to his simulation results. In addition, he collected experimental data of the lift generated by a boomerang with rotational and translational speed while immersed in a water tank. One of the key conclusions of Hess's work is that the non-dimensional lift coefficient generated by the boomerang is proportional to the *square* of the non-dimensional rotational speed. This is referred to as Hess's model. In 2012, Vassberg made a significant leap forward by using blade element theory to drive expressions for lift, rolling-moment, and pitching-moment [2]. The equations Vassberg developed predict that the non-dimensional lift coefficient generated by the boomerang is proportional to a *constant plus square* of the non-dimensional rotational speed. This is referred to as Vassberg's model in this paper. In 2019,

we extended Vassberg's work to include the effect of reversal of airflow and reversal of angle of attack and concluded that non-dimensional lift coefficient is *linearly* proportional to the non-dimensional rotational speed [3].

This paper is organized as follows. In section II, we expressed the non-dimensional lift coefficient of Hess, Vassberg and Gudem in terms of blade pitch and angle-of-incidence. These expressions are then simplified for the useful region of the non-dimensional rotational speed, $0 < \chi < 1$. In section III, we describe the wind tunnel equipment and the procedure used to measure lift at various rotational speeds, translational speeds, blade pitches and angles-of-incidence. In section IV, we compare the wind tunnel measurements with theoretical predictions of Hess [1], Vassberg [2] and Gudem [3]. Section V provides the conclusions.

II. Lift and Non-Dimensional Lift Coefficients

In this derivation, the body axis coordinate system of the boomerang will be used. The rotation angle, ψ, begins at the y axis and goes around in the counterclockwise direction. The boomerang is assumed to have its translational velocity in the x-z plane.

The equation for lift as a function of ψ of a differential blade segment can be expressed as:

$$dL(\psi, r) = \frac{1}{2}\rho C V_{no}^2 (C_{lo} + \alpha_{AOA} C_{l\alpha}) dr \tag{1}$$

where ρ is the density of air, C is the chord of the blade, V_{no} is the velocity along the airfoil, C_{lo} is the coefficient of basic lift for the airfoil, α_{AOA} is the angle of attack of the airfoil to the oncoming wind, $C_{l\alpha}$ is the coefficient of angle of attack lift for the airfoil, and r is the distance from the center of the boomerang (on the blade). As described in [2], this expression must be split into two lifts: one for when wind is hitting the leading edge of the blade element, $dL^+(\psi, r)$, and another for the trailing edge, $dL^-(\psi, r)$,

$$dL^+(\psi, r) = \frac{1}{2}\rho C V_{no}^2 (C_{lo+} + \alpha_{AOA} C_{l\alpha+}) dr \tag{2.a}$$

$$dL^-(\psi, r) = \frac{1}{2}\rho C V_{no}^2 (C_{lo-} + \alpha_{AOA} C_{l\alpha-}) dr \tag{2.b}$$

where C_{lo+} and $C_{l\alpha+}$ are the coefficients of basic lift and lift due to angle of attack for the leading edge, respectively, while C_{lo-} and $C_{l\alpha-}$ are those for the trailing edge. dL^+ is valid in the region $0 < \psi < \pi - \cos^{-1}\left(\frac{r\chi}{R}\right)$, and dL^- is valid in the region $\pi - \cos^{-1}\left(\frac{r\chi}{R}\right) < \psi < \pi$. Averaging (2.a) and (2.b) over ψ and integrating with respect to r gives the average lift generated over the leading and trailing portions of the entire blade:

$$\overline{L^+} = \frac{1}{2}\rho C \left[C_{lo+} \int_0^R \frac{1}{\pi} \int_0^{\pi - \cos^{-1}\left(\frac{r\chi}{R}\right)} V_{no}^2 \, d\psi \, dr + C_{l\alpha+} \int_0^R \frac{1}{\pi} \int_0^{\pi - \cos^{-1}\left(\frac{r\chi}{R}\right)} \alpha_{AOA} V_{no}^2 \, d\psi \, dr \right] \tag{3.a}$$

$$\overline{L^-} = \frac{1}{2}\rho C \left[C_{lo-} \int_0^R \frac{1}{\pi} \int_{\pi - \cos^{-1}\left(\frac{r\chi}{R}\right)}^{\pi} V_{no}^2 \, d\psi \, dr + C_{l\alpha-} \int_0^R \frac{1}{\pi} \int_{\pi - \cos^{-1}\left(\frac{r\chi}{R}\right)}^{\pi} \alpha_{AOA} V_{no}^2 \, d\psi \, dr \right] \tag{3.b}$$

The α_{AOA} contains the information of the blade pitch, α_p, and the angle-of-incidence, α_{AOI}. As shown in [2], for small blade pitches and angle-of-incidences, the angle-of-attack can be expressed as

$$\alpha_{AOA} \approx \frac{\alpha_p(V cos\psi + r\omega) + \alpha_{AOI} V}{|V cos\psi + r\omega|} \tag{4}$$

The Expression for Total Average Lift, $\bar{L}$

Substituting (4) into (3.a) and (3.b) gives the expressions for average lift over the leading and trailing edges:

$$\overline{L^+} = \frac{1}{2}\rho C\left[C_{lo+}\int_0^R \frac{1}{\pi}\int_0^{\pi-\cos^{-1}\left(\frac{r\chi}{R}\right)} V_{no}^2\, d\psi\, dr + \alpha_p C_{l\alpha+}\int_0^R \frac{1}{\pi}\int_0^{\pi-\cos^{-1}\left(\frac{r\chi}{R}\right)} V_{no}^2\, d\psi\, dr + \alpha_{AOI} C_{l\alpha+} V\int_0^R \frac{1}{\pi}\int_0^{\pi-\cos^{-1}\left(\frac{r\chi}{R}\right)} |V_{no}|\, d\psi\, dr\right] \tag{17}$$

$$\overline{L^-} = \frac{1}{2}\rho C\left[C_{lo-}\int_0^R \frac{1}{\pi}\int_{\pi-\cos^{-1}\left(\frac{r\chi}{R}\right)}^{\pi} V_{no}^2\, d\psi\, dr - \alpha_p C_{l\alpha-}\int_0^R \frac{1}{\pi}\int_{\pi-\cos^{-1}\left(\frac{r\chi}{R}\right)}^{\pi} V_{no}^2\, d\psi\, dr + \alpha_{AOI} C_{l\alpha-} V\int_0^R \frac{1}{\pi}\int_{\pi-\cos^{-1}\left(\frac{r\chi}{R}\right)}^{\pi} |V_{no}|\, d\psi\, dr\right] \tag{18}$$

where the negative sign in front of the α_p term in (18) is from the sign change of $V cos\psi + r\omega$ over the trailing edge region of flow in (4). To make (17) and (18) more compact, we define

$$L_p^+ = \frac{1}{V^2 R}\int_0^R \frac{1}{\pi}\int_0^{\pi-\cos^{-1}\left(\frac{r\chi}{R}\right)} V_{no}^2\, d\psi\, dr \tag{19.a}$$

$$L_p^- = \frac{1}{V^2 R}\int_0^R \frac{1}{\pi}\int_{\pi-\cos^{-1}\left(\frac{r\chi}{R}\right)}^{\pi} V_{no}^2\, d\psi\, dr \tag{19.b}$$

$$L_{AOI}^+ = \frac{1}{VR}\int_0^R \frac{1}{\pi}\int_0^{\pi-\cos^{-1}\left(\frac{r\chi}{R}\right)} |V_{no}|\, d\psi\, dr \tag{19.c}$$

$$L_{AOI}^- = \frac{1}{VR}\int_0^R \frac{1}{\pi}\int_{\pi-\cos^{-1}\left(\frac{r\chi}{R}\right)}^{\pi} |V_{no}|\, d\psi\, dr \tag{19.d}$$

where L_p^+ is the nondimensional integral corresponding to the blade pitch over the leading edge, L_p^- is that which is over the trailing edge, L_{AOI}^+ is the nondimensional integral corresponding to the angle-of-incidence over leading edge, and L_{AOI}^- is that which is over the trailing edge. Substituting the nondimensional integrals defined in (19) into (17) and (18), and summing gives the total average lift of the blade in one rotation:

$$\bar{L} = \overline{L^+} + \overline{L^-}$$

$$= \frac{1}{2}\rho C R V^2\left[C_{lo+}L_p^+ + C_{lo-}L_p^- + \alpha_p\left(C_{l\alpha+}L_p^+ - C_{l\alpha-}L_p^-\right) + \alpha_{AOI}\left(C_{l\alpha+}\, L_{AOI}^+ + C_{l\alpha-}L_{AOI}^-\right)\right] \tag{22}$$

where the bracketed term in (22) is the non-dimensional coefficient of total lift, $\bar{C}_l$.

Combining Basic Lift and Lift Due to Blade Pitch

In $\bar{C}_l$, the basic and pitch terms may be combined since they both depend on L_p^+, and L_p^-. Taking $\alpha_{AOI} = 0$ since it does not factor into this analysis, $\bar{C}_l$ becomes

$$\overline{C_l}(\alpha_{AOI}=0)=\left(C_{lo+}+C_{l\alpha+}\alpha_p\right)L_p^+ +\left(C_{lo-}-C_{l\alpha-}\alpha_p\right)L_p^- \tag{23}$$

This is the simplest expression for $\overline{C_l}$, since Li_p^+ and Li_p^- are not combinable. The terms multiplying the nondimensional integrals Li_p^+ and Li_p^- may be interpreted as the equations of lines. The variable is α_p, the slopes are $C_{l\alpha+}$ and $-C_{l\alpha-}$, and the intercepts are C_{lo+} and C_{lo-}. Each equation is synonymous to the equation for the lift coefficient of a cambered (top-down asymmetric) airfoil.

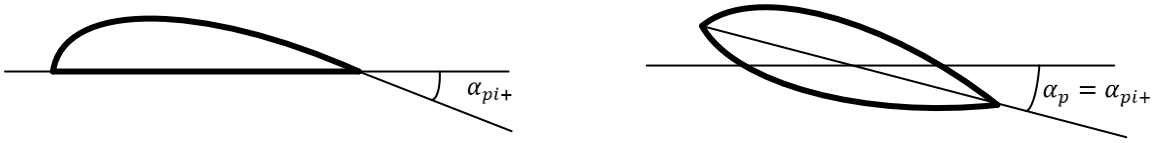

Figure 2: Illustration of the inherent pitch angle of a cambered airfoil and the blade pitch of a symmetric airfoil

It is well known that the lift generated by a cambered airfoil is approximately equivalent (for small α_p) to that generated by a top-down symmetric airfoil at a blade pitch equal to the inherent blade pitch of the cambered airfoil (Fig. 2). If the cambered airfoil is aligned parallel to the direction of the wind, then its inherent blade pitch is the angle one must rotate the cambered airfoil to achieve zero lift. Therefore, the intercept, C_{lo+}, may be replaced by the inherent blade pitch of the leading edge of the cambered airfoil, α_{pi+}, times the slope of the line, $C_{l\alpha+}$. Similarly, the intercept, C_{lo-}, may be replaced by the inherent blade pitch over the trailing edge of the cambered airfoil, α_{pi-}, times the slope of the line, $C_{l\alpha+}$. Thus, $\overline{C_l}$ becomes

$$\overline{C_l}(\alpha_{AOI}=0)=C_{l\alpha+}(\alpha_{pi+}+\alpha_p)L_p^+ +C_{l\alpha-}(\alpha_{pi-}-\alpha_p)L_p^- \tag{24}$$

Evaluation of the Non-Dimensional Lift Coefficients

The boomerang used in the wind tunnel experiments has top-down symmetry, so in this paper we will take $\alpha_{pi+}=\alpha_{pi-}=0$. Thus, including the α_{AOI} term, the non-dimensional lift coefficient is

$$\overline{C_l}=C_{l\alpha+}\left[\alpha_p\left(L_p^+-\frac{C_{l\alpha-}}{C_{l\alpha+}}L_p^-\right)+\alpha_{AOI}\left(L_{AOI}^+ +\frac{C_{l\alpha-}}{C_{l\alpha+}}L_{AOI}^-\right)\right] \tag{25}$$

Evaluating the non-dimensional integrals in (25) results in a complicated function of χ that can be simplified by considering how real boomerangs almost always operate with $0<\chi<1$, and so only small values of χ need to be compared to experiment. Therefore, we may expand (25), giving:

$$\overline{C_l}\approx C_{l\alpha+}\left[\alpha_p\left(\frac{1+C_{l\alpha-}/C_{l\alpha+}}{\pi}\chi\right)+\alpha_{AOI}\left(\frac{1+C_{l\alpha-}/C_{l\alpha+}}{\pi}\right)\right] \tag{26}$$

This is the non-dimensional lift coefficient predicted by Gudem [3]. For small χ, it is strongly linear. The expanded non-dimensional lift coefficient calculated by Vassberg [2] can be found by disregarding the reversal of pitch during trailing edge flow. It has a similar form to Gudem's prediction:

$$\overline{C_l}\approx C_{l\alpha+}\left[\alpha_p\left(\frac{1}{2}+\frac{\chi^2}{3}\right)+\alpha_{AOI}\left(\frac{2}{\pi}\right)\right] \tag{27}$$

but is quadratic for small χ. Finally, Hess' aerodynamic model [1] predicts:

$$\overline{C_l} = h\chi^2 \tag{28}$$

where h is an experimental constant.

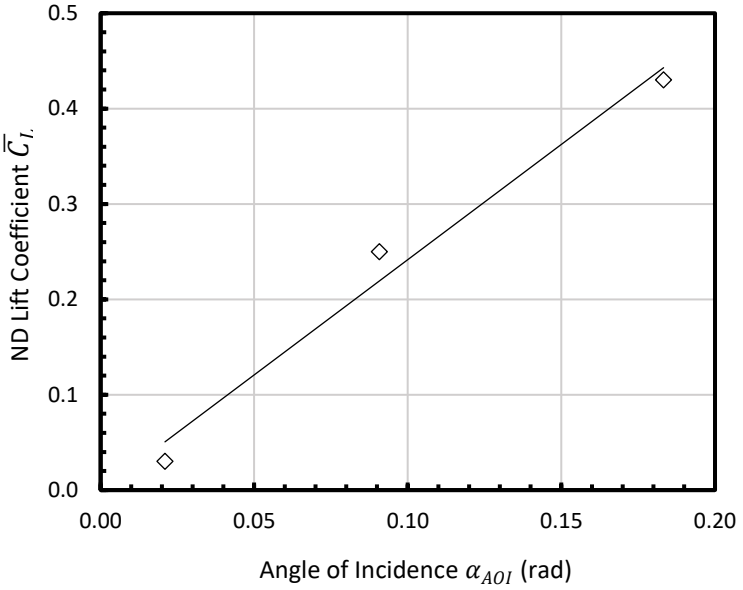

Figure 3: Measured ND Lift Coefficient ($\overline{C_l}$) Vs. Angles-of-Incidence (α_{AOI}) at $\chi = 0$

The ratio $C_{l\alpha-}/C_{l\alpha+} = 3/4$ was determined by taking the ratio between lift measured for the boomerang spinning in the positive and negative directions. The constant $C_{l\alpha+} = 4.5$ was found by considering the behavior of the measured $\overline{C_l}$ at $\chi = 0$ against various values of α_{AOI}. The resulting curve (Fig. 3) was compared to (26) at $\chi = 0$:

$$\overline{C_l}(\chi = 0) = C_{l\alpha+}\left(\frac{1 + C_{l\alpha-}/C_{l\alpha+}}{\pi}\right)\alpha_{AOI} \tag{29}$$

which correctly predicts that the curve is linear with slope $C_{l\alpha+}\left(\frac{1+C_{l\alpha-}/C_{l\alpha+}}{\pi}\right)$. The constant h was determined by providing the best fit curve while maintaining a realistic slope.

III. Wind Tunnel Setup

The boomerang used for the measurements is the VIPAR (Variable Inclination Pitch Angle Rang) shown in Fig. 4. It is composed of four separate aviation grade plywood arms shaped with a top-down symmetry. The arms are attached to a boss mounted on a spindle so that the blade pitch of each arm can be adjusted. The blade pitch is measured photographically with an accuracy of 0.2°. Each arm has a 30mm chord and a 5mm maximum thickness. The radius of the boomerang is 13cm.

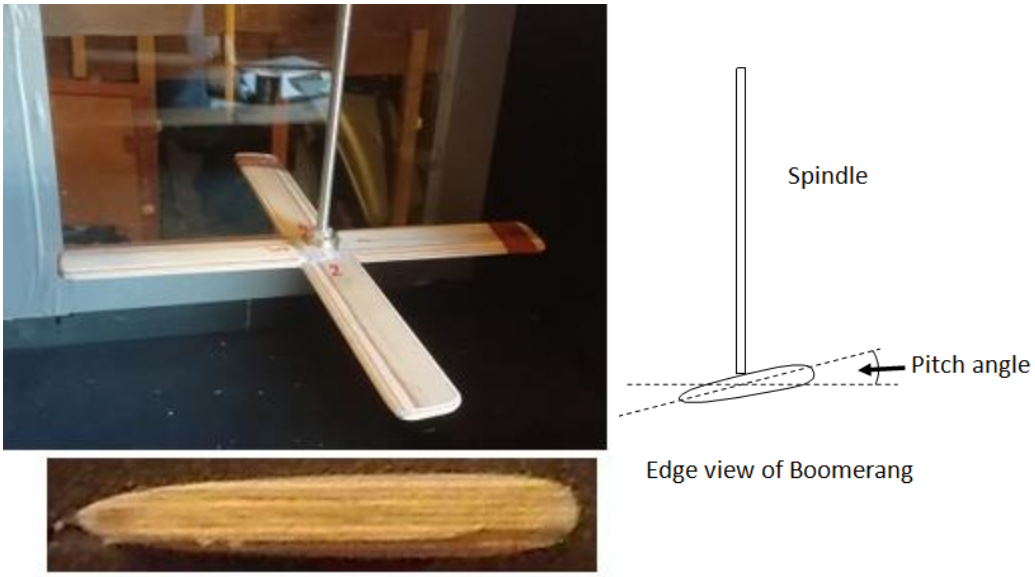

Figure 4: The VIPAR Boomerang, Airfoil Symmetry and Blade Pitch

A compact wind tunnel of length 7m was used to find the lift force produced by the rotating VIPAR at different incident angles to the air stream as shown in Fig. 5. The wind tunnel was especially constructed to allow a spinning boomerang to be suspended in the middle of a test section. The test section is 500mm in length and its rectangular cross section has a 350mm height and 400mm width.

The boomerang is attached to a 6mm diameter steel spindle passing out of the tunnel through a small hole and is driven by a 12V variable speed motor that can rotate up to 28rps. The wind speed in the tunnel itself is also variable with a maximum of 14m/s.

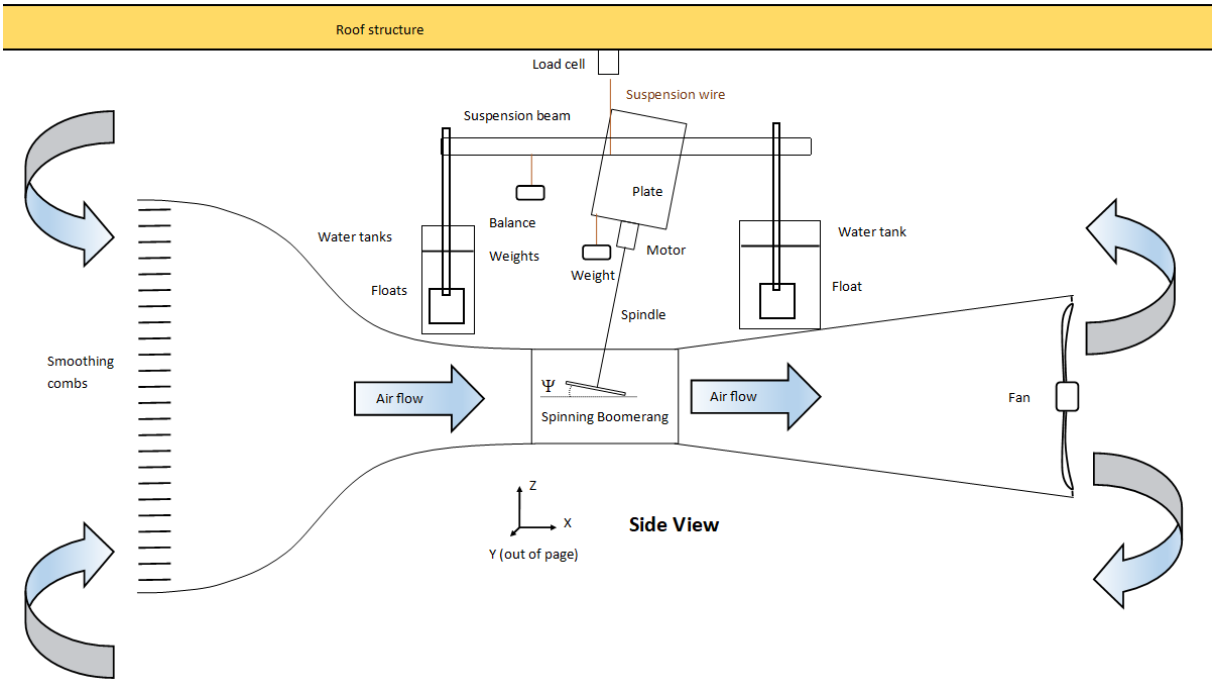

Fig. 5: Wind Tunnel Used to Measure Boomerang Lift

The VIPAR and motor are mounted on a plate that allows the boomerang to be inclined at varying angles-of-incidence (α_{AOI}) to the air stream from a suspension beam. The suspension beam is held aloft by a wire suspended from the roof structure and kept level with balance weights. The suspension beam can also be pulled in the X direction by drag forces on the boomerang. Lift forces are measured by a load cell holding the suspension beam above the center of the boomerang. Additionally, 3 water tanks and floats help to balance the weight of the motor and have the added benefit of vibration damping and reducing the load on the suspension beam. Anchor screws and wires are used for resisting drag forces produced in the X direction.

The load cell data was collected from a Phidget bridge and digitally averaged over an interval of 20s for each measurement.

Experimental Procedure

Each series of tests started with the plane of the boomerang set at an angle-of-incidence to the airflow which was measured with a digital inclinometer to an accuracy of about 0.5°. The boomerang was aligned in the middle of the tunnel with the suspension beam horizontal and oriented so that the spindle was solely in the X-Z plane. The load cell was calibrated and zeroed prior to inducing the airflow and spinning the boomerang.

The wind speed was adjusted and measured from a digital anemometer mounted in the tunnel approximately 150mm upstream of the boomerang. The spin of the boomerang was adjusted and recorded from a calibrated reed switch sensor or light beam and oscilloscope. For each combination of wind speed and spin rate, the load cell measurements of lift force were recorded. Approximately 200 tests (with several load cell measurements for each test) were taken.

IV. Results

Wind tunnel measurements of lift were conducted for $\alpha_p = 5.5°$ and three angles of incidence. Figs 6, 7, and 8 correspond to $\alpha_{AOI} = 1.2°$, $\alpha_{AOI} = 5.2°$, and $\alpha_{AOI} = 10.5°$, respectively. Figs. 6 a), 7 a), and 8 a) show measurements of lift as a function of rotational speed for various wind tunnel speeds. Also included are best fit lines to emphasize the quadratic or linear nature of the trends. Figs. 6 b), 7 b), and 8 b) depict the measured ND lift coefficient as a function of the ND rotational speed and the predicted trends of Hess [1], Vassberg [2], and Gudem [3]. We only consider the useful region of the ND rotational speed ($0 < \chi < 1$).

Fig. 6 a) suggests that the measured lift has a strong linear dependence on the rotational speed for constant higher wind speeds, $L \propto V\omega$. Since high wind speeds correspond to values of χ in the useful region, we expect that $\overline{C}_L$ be linear in χ as well. This is because $L \propto V^2\bar{C}_L$, and so $\overline{C}_L \propto \chi = \frac{R\omega}{V}$ yields $L \propto V\omega$. Analyzing Fig. 6 b) reveals that $\overline{C}_L$ is most likely linear in χ, since the measurements closely follow the linear prediction of Gudem (26). Vassberg's trend (27) vastly overpredicts the y-intercept and its quadratic nature does not accurately represent the data. Hess's prediction (28) has a realistic y-intercept; however, it is quadratic and thus does not fit the measured data well.

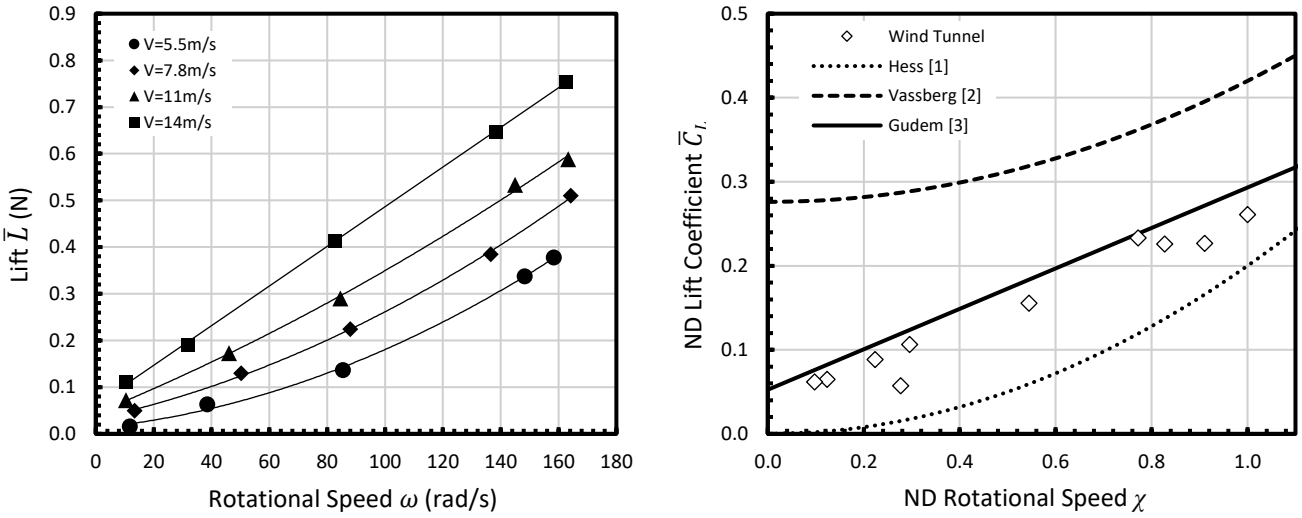

Figure 6: a) Measured Lift $(\overline{L})$ Versus Rotational Speed (ω) for $\alpha_p = 5.5°$ and $\alpha_{AOI} = 1.2°$, b) Measured and Predicted ND Lift Coefficient $(\overline{C}_L)$ Versus ND Rotational Speed (χ) for $\alpha_p = 5.5°$ and $\alpha_{AOI} = 1.2°$

Fig. 7 a) again depicts that the lift is linear with respect to the rotational speed for high wind speeds. The graph also clearly shows that the trends have a nonzero y-intercept. This is because although the rotational speed is zero at the intercept, the wind speed is not and so the boomerang will still produce lift. The linear trend and y-intercept are closely predicted by Gudem [3] in Fig. 7 b), however, there is some deviation towards Vassberg's [2] prediction as χ becomes larger. This is likely due to experimental error. Vassberg [2] and Hess [1] overpredict and underpredict the y-intercept, respectfully, and both predict quadratic trends that do not quite match the data.

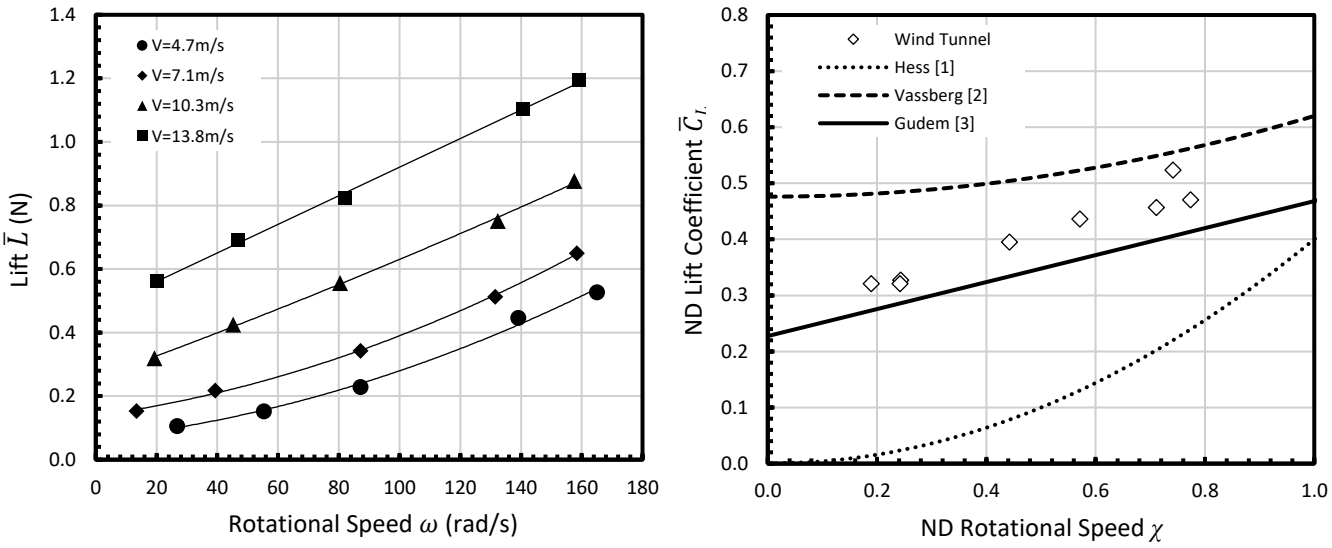

Figure 7: a) Measured Lift $(\bar{L})$ Versus Rotational Speed (ω) for $\alpha_p = 5.5°$ and $\alpha_{AOI} = 5.2°$, b) Measured and Predicted ND Lift Coefficient $(\bar{C}_L)$ Versus ND Rotational Speed (χ) for $\alpha_p = 5.5°$ and $\alpha_{AOI} = 5.2°$

Figs. 8 a) and 8 b) show that the measurements in the useful region of χ are linear with a higher y-intercept, both of which Gudem [3] predicts accurately. Vassberg's [2] and Hess' [1] quadratic trends overpredict and underpredict the y-intercept, respectfully, and thus do not match the data well.

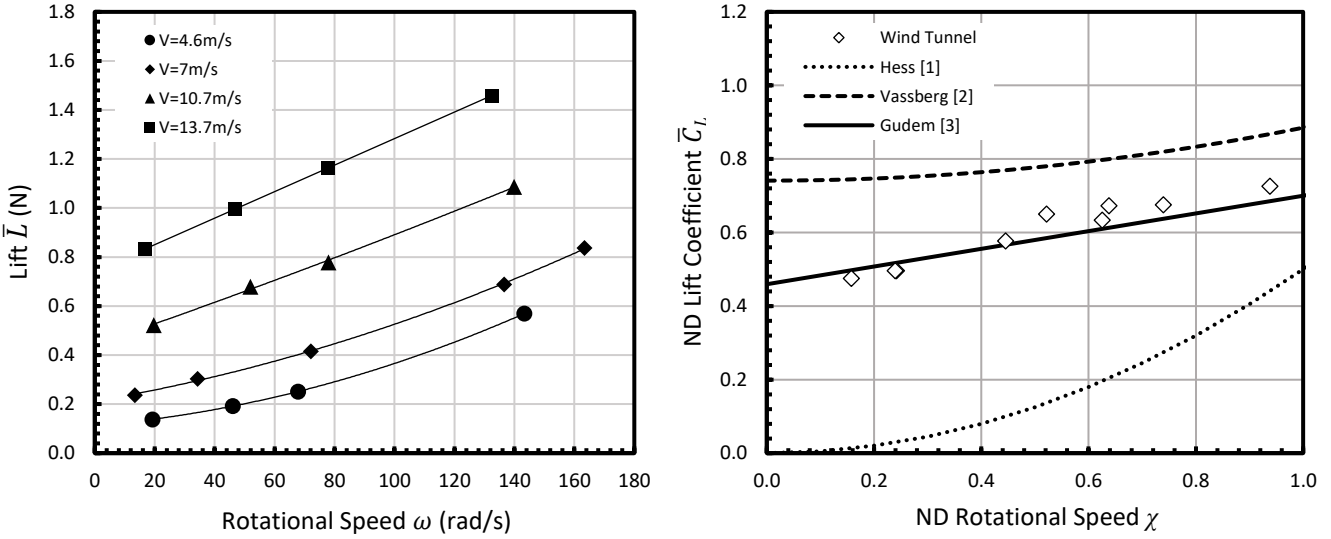

Figure 8: a) Measured Lift $(\bar{L})$ Versus Rotational Speed (ω) for $\alpha_p = 5.5°$ and $\alpha_{AOI} = 10.5°$, b) Measured and Predicted ND Lift Coefficient $(\bar{C}_L)$ Versus ND Rotational Speed (χ) for $\alpha_p = 5.5°$ and $\alpha_{AOI} = 10.5°$

Therefore, the measured ND lift coefficient seems to follow the Gudem's prediction (26), behaving linear in χ. This not only validates the use of Blade Element Theory to describe the lift of boomerangs, but also shows how the reversal of airflow over the trailing edge contributes significantly to the lift.

V. Conclusion

The analytical expressions for the ND lift coefficient developed by Hess [1], Vassberg [2], and Gudem [3] were compared to measurements conducted in a wind tunnel. The results show that the ND lift coefficient is approximately linear as a function of the ND rotational speed, matching Gudem's prediction (26). This implies that considering the reversal of airflow over the trailing edge is necessary to develop an accurate model for the lift of boomerangs. Future work will involve comparing the moments and drag experienced by boomerangs to wind tunnel experiments.

References

[1] F. Hess, "Boomerangs, Aerodynamics and Motion," Ph.D. Thesis, Groningen University, June 1975.

[2] John Vassberg, "Boomerang Flight Dynamics," 30th AIAA Applied Aerodynamics Conference, 2012.

[3] P. Gudem, M. Schütz, and K. Holland, "Flight Dynamics of Boomerangs: Impact of reversal of airflow and reversal of angle of attack", AIAA Aviation Forum and Exposition, 2019.

[4] P. Gudem, M. Laslett, G. Carfano, M. Schütz, K. Holland and H. Murguia, "Flight Dynamics of Boomerangs: Impact of Drag Force and Drag Torque", AIAA Aviation Forum and Exposition, 2020.

Biography

Justin Tahmassebpur is currently an undergraduate at the University of California, San Diego studying engineering physics. He is especially interested in mathematical modeling and theoretical physics. After he graduates, he will begin a PhD in applied physics at Cornell University.

Martin Laslett graduated with a B.Sc. in physics from the University of Leeds in 1984 and M.Sc. degree in 1980 from Aston University. For his M.Sc. thesis, whilst at Aston University, he developed a graphical boomerang simulator (BOOMLAB) in 1984 to predict the 3-dimensional flight trajectory of editable boomerang shapes. Martin was also the editor of British boomerang society magazine for several year. He wrote the Essential Boomerang Book to explain some of the current theories of boomerang behavior to a wider audience. He constructed the carbon fiber boomerang that holds the Guinness World Record for the largest returning boomerang. Martin is the current British boomerang throwing champion and has competed in many world boomerang competitions over the past 20 years. He has constructed two amateur wind tunnels specifically for boomerang testing, with horizontal and vertical air flow and documents any boomerang related science on the website http://Boomlab.org. Martin works as an IT trainer in the UK for Quanta Training Ltd.

Manuel Schütz received his degree (lic.phil.nat) in physics from the Institute of Applied Physics, University of Bern, Bern, Switzerland in 2003. He is a five-time World Champion in boomerang throwing and holds several world records, among them the long-distance world record (apex at 238m). Since 2009, he is a mathematics and science teacher at WKS KV Bildung in Bern (Federal Vocational Baccalaureate).

Prasad Gudem received the B. Tech degree in Electrical Engineering from the Indian Institute of Technology, Madras, India, in 1988, and the Ph.D. degree in Electrical Engineering from the University of Waterloo, Waterloo, Ontario, Canada, in 1996. He was a Vice President of Engineering at Qualcomm from 2014-2018 and currently an Adjunct Professor in the Department of Electrical and Computer Engineering, University of California at San Diego, La Jolla, CA, USA. He has 50+ patents and 40+ IEEE publications. He taught several graduate-level classes and co-advised twelve Ph.D. students in RF integrated circuit (IC) design. Dr. Gudem was the recipient of the Graduate Teaching Award in recognition of his outstanding teaching of the ECE265 course sequence, “Communication Circuit Design: I, II, and III”. He is an avid follower of the history of STEM (Science, Technology, Engineering, and Mathematics).